Vacancy-Driven Twinning in Metal Nanoparticles: From Bulk Morphology Transformation to Optical and Electrochemical Effects

Ilia Smirnov [a] *, Zbigniew Kaszkur [b] *, Mohit Chaudhary [c,d], Hans-Christian Weissker [c,d], Riccardo Ferrando [e], Pawel Kulesza [a]

[a] University of Warsaw, Warsaw, Poland.

[b] Institute of Physical Chemistry, Warsaw, Poland.

[c] Aix-Marseille University, CNRS, CINaM UMR 7325, 13288 Marseille, France

[d] European Theoretical Spectroscopy Facility https://www.etsf.eu.

[e] University of Genoa, Genoa, Italy

* Correspondence and requests for materials should be addressed to I.S. (email: snowwhiteman42@gmail.com) or Z.K. (email: zkaszkur@ichf.edu.pl)

Note S 1

Characterization of simulated multidomain nanoparticles is not a trivial task. We highlight four general methods for morphology evaluation.

a) Elastic strain analysis embedded into OVITO software [1]. This analysis determines the imaginary strain-free translation vector of the ideal fcc crystal structure and compares it with the analyzed elastically strained model. The local transformation tensor (from ideal to strained models) represents information about deformations. The crystal structure analysis is based on the same principle but considers the second neighbor shell, which allows differentiation between fcc and hcp structures.

This method is visually attractive. The drawback is that it fails when an analyzed particle is populated with vacancies. The first step in elastic strain/structure calculations is analyzing the number of atoms neighboring the given one. Once it is located close to vacancies, the neighbor analysis fails, and it is impossible to determine to which crystal structure the given atom belongs. Therefore, models with a high concentration of vacancies remain poorly characterized (**Fig. S1** a). Nevertheless, the algorithm can be improved later.

b) Visual estimation. The ideal fcc domain is a crystal structure without twin or stacking faults. Therefore, one can estimate the borders of fcc domains by looking at the ordering of raws of atoms in 3D software (like Blender).

This method is only approximate and can be used for only slightly disordered models. However, this approach is not sensitive to vacancies and allows the description of models that can not be characterized with the first approach (**Fig. S1** b).

c) MDXRD

The multidomain XRD approach allows for determining the average size and number of domains in a given cluster [2]. This method is based on the fact that once two ideal fcc segments are connected by a twin plane, the ratio of diffraction peak heights (111 to 200 or 220 peaks) changes. The more domains there are, the smaller the ratio will be.

In experimental samples, this method requires meticulous adjustment of the background line. However, in the case of simulated models, this is not a problem. MDXRD allows numerical characterization of complex randomly twinned multidomain structures populated with vacancies. Unlike the elastic strain analysis (method a) MDXRD is based on the analysis of XRD patterns calculated from the Debye equation. Therefore, the multidomain approach is not algorithm-dependent characterization as the elastic strain calculator. Moreover, it is straightforward and can be applied to real-life samples. Consequently, it was used as a primary tool in the current article.

Analysis of the relaxed CUB 5083 + 14% of vacancies (**Fig. S1**) with MDXRD estimates the number of domains as equal to 1.9. The number of domains is not an integer because diffraction techniques estimate the contributions of each domain into a total diffraction pattern. In the case of ideal DEC and ICO, the number of domains is an integer (5 and 20 corresponding) because their domains are equal in size.

However, in randomly twinned NPs the bulk morphology is more complex. As we can see from **Fig. S1** b (CUB 5083 + 14%) the model consists of roughly three domains: a large (66%), one medium (30%), one tiny segment (2%), and other atoms (2%). Although there are three physical segments, their contributions to diffraction patterns are not equal. According to the Laue formula, diffraction peak height is proportional to the square of a number of atoms in a given direction. Roughly, the scattering peak height of the large domain (66% of atoms) is (66^2) / (30^2) = 4.84 higher than that of the medium-sized domain (30% of atoms). Therefore, the contribution of a large domain is more significant.

The mathematical formula describing the meaning of the number of domains can be expressed in the following way:

$$Number\ of\ domains\ = \frac{1}{\left[\frac{\sum_{domain\ number}^{1} (atoms\ in\ a\ domain\ ^2)}{total\ number\ of\ atoms\ ^2}\right]}$$

Applying the above-given formula to the CUB 5083 + 14% vacancies model (**Fig. S1**); one can estimate the number of domains. The obtained value is in agreement with the one obtained by MDXRD.

$$Number\ of\ domains = \frac{1}{\left[\frac{66^2 + 30^2 + 2^2 + 2^2}{100^2}\right]} \cong 1.899$$

d) Machine learning

Another approach relies on machine learning of atomic dynamics and statistical surface identification [3].

Note S 2

For CUBs consisting of 21127 and 28741 atoms, the effect of 22% of vacancies is not described because of the extensive computational time.

Note S 3

The multidomain model shown in Fig. 3 of the main article consists of 4 domains: 612, 408, 512, and 525 atoms. In total, it is 2057 atoms like in the perfect, one domain, closed shell CUB. Therefore both models can be compared directly without any adjustment.

However, the 2057 atom configuration is not optimal for the 4-domain structure. Due to the readjustment of domains, some surface layers tend to shift from their optimal position, creating additional strain on the two domains. The most stable form for a 4-domain cluster of similar size

is a cluster made of 1976 atoms with potential energy per atom equal to -3.6745 [eV/at.] (calculated from the Cluster software with Sutton-Chen potentials).

To estimate the stability of such a structure, one can rescale the energy of CUBs to 1976 atoms. The potential energy per atom of ideal CUBs made of 2057 and 1415 atoms is equal to -3.6763 and -3.6624 [eV/at.], respectively. The potential energy per atom of the 1-domain 1976 atom cluster is equal to ~ -3.6745[eV/at.].

The comparison of the ideal 4-domain structure with the rescaled energy of CUBs shows that the stability of both structures is nearly identical. The cohesive energy of an atom mostly depends on the distance in the first coordination shell and does not differ between fcc and hcp arrangements (and for atoms laying on stacking planes). So the energy differences are related mostly to the surface structure (appearance of steps) or to atoms at the intersection of the twinning planes.

Supplementary Data

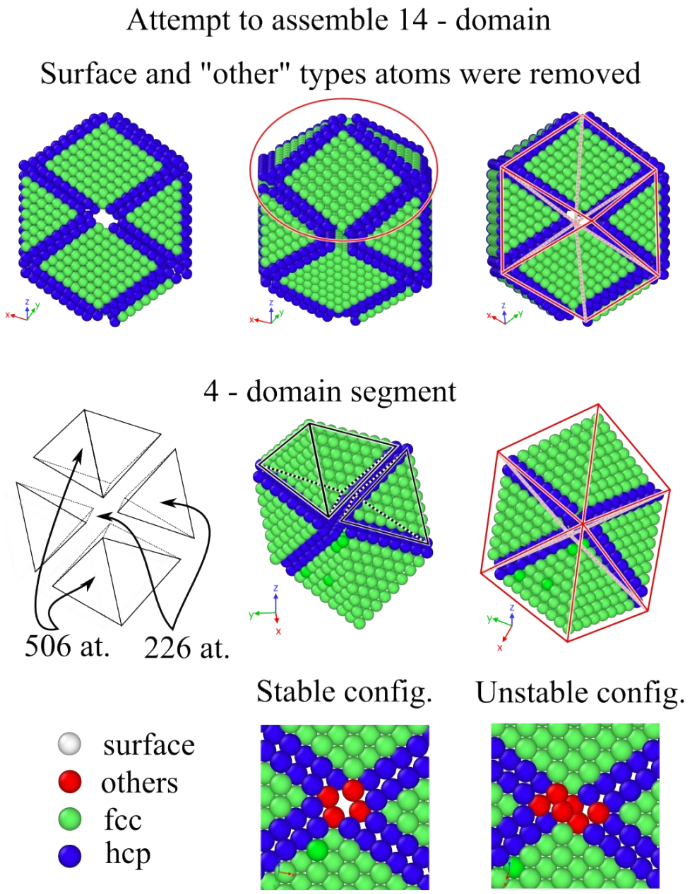

Data S1 The scheme of 14 domain structure assembly from pyramids and tetrahedrons. In the low right corner are two types of hcp cross-twinning: stable and unstable.

The manual positioning of segments is not a trivial and routine task. Adjusting segments in 2D is rather straightforward while adjusting in 3D becomes more complex. Positioning fcc domains one by one to create a stable hcp cross-twinning pattern is possible only for up to 10-12 domains. The addition of the last domains results in the appearance of unstable hcp cross-twinning patterns.

During the relaxation of the obtained 14-domain structure, this unstable cross-twinning becomes a center of ordering. In other words, starting from the unstable crossing, nearby hcp layers begin to rearrange into fcc. At the next stage, not only neighboring but other hcp layers start to restructure into fcc.

It seems that 14 domain structures can be stable only if all cross-twinning on corners are reassembled in a stable configuration. However, it is not clear whether it is possible in general.

Data S2 The shown in Figure 4 model was made from fcc ball consisting of 5089 atoms with 22% of atoms randomly deleted, then energy relaxed, so the final number of atoms is equal to 3969. Let's find the energy per atom for the same size CUB, DEC (Marks decahedron with m=n, p=3 [4]), and ICO.

	CUB		DEC		ICO	
	atoms	E / at.	atoms	E / at.	atoms	E / at.
Regular model	5083	-3.703	4776	-3.706	5083	-3.699
	3871	-3.696	3594	-3.699	3871	-3.692
Linear rescale	3969	-3.697	3969	-3.701	3969	-3.693

Supplementary Table

Change of density (SAXS)

TEMP, K	Vacancies [%]; MD + relaxation								
	0	8	10	12	14	16	18	20	22
0	21.9	19.7	19.3	18.9	19.4	20.2	20.4	20.8	21.0
300	21.9	20.1	19.9	20.8	20.9	20.7	21.0	21.1	21.3
350	21.9	20.2	19.9	20.8	20.9	20.8	21.1	21.1	21.4
400	21.9	20.3	19.9	20.9	20.9	20.9	21.4	21.1	21.4
450	21.9	20.5	20.1	21.1	21.0	21.0	21.3	21.2	21.5
500	21.9	20.9	20.4	21.3	21.2	21.1	21.2	21.2	21.5
550	21.9	21.0	20.5	21.5	21.3	21.1	21.4	21.3	21.6
600	21.9	21.3	20.9	21.7	21.5	21.4	21.5	21.6	21.8
650	21.9	21.4	21.3	21.7	21.6	21.5	21.6	21.7	21.8
700	21.9	21.5	21.4	21.7	21.8	21.7	21.7	21.7	21.9
750	21.8	21.6	21.6	21.8	21.8	21.7	21.8	21.8	21.9
800	21.6	21.8	21.7	21.7	21.9	21.6	21.9	21.8	21.5

Number of domain
18.87
19.19
19.51
19.83
20.15
20.47
20.79
21.95

Table S1 MD heating of a 5089-atom fcc sphere with 0-22% VAC followed by relaxation. Densities (N) of models were calculated based on simulated SAXS patterns (q range 0.01 to 0.28 $Å^{-1}$).

Change of size (SAXS)

TEMP, K	Vacancies [%]; MD + relaxation								
	0	8	10	12	14	16	18	20	22
0	27.38	27.18	27.09	27.01	26.61	26.07	25.90	25.55	25.39
300	27.38	27.12	26.87	26.53	26.23	26.04	25.79	25.49	25.28
350	27.38	27.12	26.87	26.53	26.22	26.04	25.79	25.49	25.26
400	27.38	27.05	26.87	26.53	26.22	26.02	25.79	25.49	25.26
450	27.38	26.94	26.86	26.50	26.21	26.02	25.78	25.49	25.26
500	27.38	26.88	26.81	26.41	26.20	26.02	25.78	25.48	25.26
550	27.38	26.86	26.78	26.39	26.20	26.02	25.75	25.49	25.24
600	27.38	26.82	26.73	26.32	26.15	25.98	25.72	25.47	25.17
650	27.38	26.80	26.68	26.31	26.16	25.94	25.71	25.45	25.17
700	27.38	26.74	26.62	26.30	26.13	25.92	25.70	25.45	25.17
750	27.39	26.70	26.56	26.29	26.11	25.89	25.66	25.42	25.16
800	27.38	26.64	26.45	26.25	26.03	25.87	25.53	25.39	25.16

Number of domain
25.16
25.47
25.79
26.11
26.43
26.75
27.07
27.39

Table S2 MD heating of a 5089-atom fcc sphere with 0-22% VAC followed by relaxation. Mean sizes (μ [Å]) of models were calculated based on simulated SAXS patterns (q range 0.01 to 0.28 $Å^{-1}$).

Number of domains (MDXRD)

TEMP, K	Vacancies [%]; MD + relaxation								
	0	8	10	12	14	16	18	20	22
0	1.0	1.1	1.2	1.3	1.5	3.3	6.6	7.9	14.5
300	1.0	1.0	1.1	1.1	1.7	3.1	4.1	4.2	6.2
350	1.0	1.0	1.1	1.1	1.7	3.3	3.4	4.3	4.6
400	1.0	1.1	1.1	1.1	1.7	3.1	3.4	4.3	4.4
450	1.0	1.4	1.1	1.1	1.7	3.0	3.5	4.2	4.5
500	1.0	1.6	1.0	1.6	1.7	3.0	3.5	4.4	5.0
550	1.0	1.6	1.0	1.0	1.7	2.8	3.4	4.3	4.9
600	1.0	1.0	1.1	1.0	1.8	2.9	1.9	4.5	2.9
650	1.1	1.1	1.1	1.1	1.9	2.7	1.6	3.8	3.0
700	1.0	1.0	1.1	1.1	1.7	2.9	1.7	3.8	2.9
750	1.1	1.2	1.2	1.4	2.3	3.8	2.0	3.9	2.7
800	3.3	2.6	3.5	7.4	4.4	6.7	5.1	6.9	10.9

Number of domain: 1, 3, 5, 7, 9, 11, 13, 15

Table S3 MD heating of a 5089-atom fcc sphere with 0-22% VAC followed by relaxation. Numbers of domains were calculated based on simulated XRD patterns analyzed by MDXRD.

Potential energy per atom [eV/atom]

TEMP, K	Vacancies [%]; relaxed models								
	0	8	10	12	14	16	18	20	22
0	-3.704	-3.656	-3.643	-3.633	-3.644	-3.665	-3.663	-3.672	-3.670
300	-3.704	-3.667	-3.664	-3.673	-3.678	-3.676	-3.677	-3.681	-3.682
350	-3.704	-3.669	-3.665	-3.674	-3.678	-3.677	-3.679	-3.681	-3.684
400	-3.704	-3.672	-3.667	-3.675	-3.679	-3.679	-3.680	-3.682	-3.684
450	-3.704	-3.676	-3.669	-3.677	-3.680	-3.681	-3.681	-3.683	-3.685
500	-3.703	-3.682	-3.674	-3.681	-3.683	-3.682	-3.682	-3.684	-3.686
550	-3.703	-3.685	-3.678	-3.685	-3.684	-3.683	-3.684	-3.686	-3.687
600	-3.703	-3.689	-3.682	-3.689	-3.688	-3.686	-3.687	-3.689	-3.690
650	-3.702	-3.690	-3.686	-3.689	-3.688	-3.689	-3.687	-3.690	-3.691
700	-3.701	-3.691	-3.687	-3.690	-3.690	-3.690	-3.688	-3.691	-3.691
750	-3.699	-3.693	-3.691	-3.691	-3.691	-3.685	-3.689	-3.690	-3.691
800	-3.695	-3.692	-3.691	-3.685	-3.690	-3.685	-3.688	-3.685	-3.679

Number of domain: -3.633, -3.643, -3.653, -3.663, -3.673, -3.683, -3.694, -3.704

Table S4 MD heating of a 5089-atom fcc sphere with 0-22% VAC followed by relaxation. Potential energies per atom were calculated by the Cluster program.

Supplementary Figures

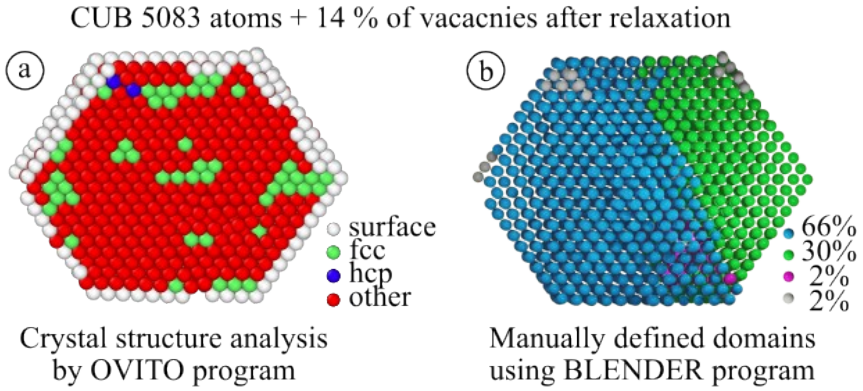

Fig. S1 Crystal phase analysis of CUB made of 5083 atoms, populated with 14% of vacancies and after relaxation using Cluster software. The analysis was performed using two approaches: a) The OVITO software utilized automatic crystal structure analysis; b) the analysis was performed manually using Blender software.

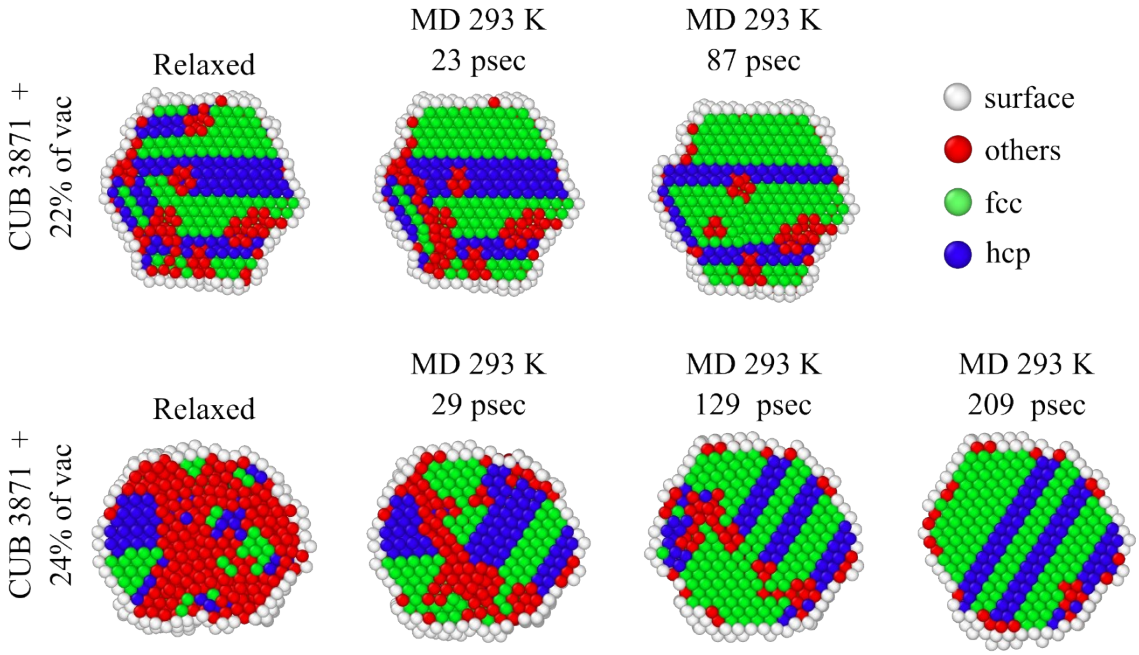

Fig. S2 MD heating simulations of relaxed multidomain clusters made of 3871 atoms CUBs populated with 22 and 24% vacancies. MD simulations were performed in Cluster software using SC potential, with a time step equal to 1 femtosecond in thermostat mode at 293 K. After heating, each model was relaxed to identify crystal structure evolution better.

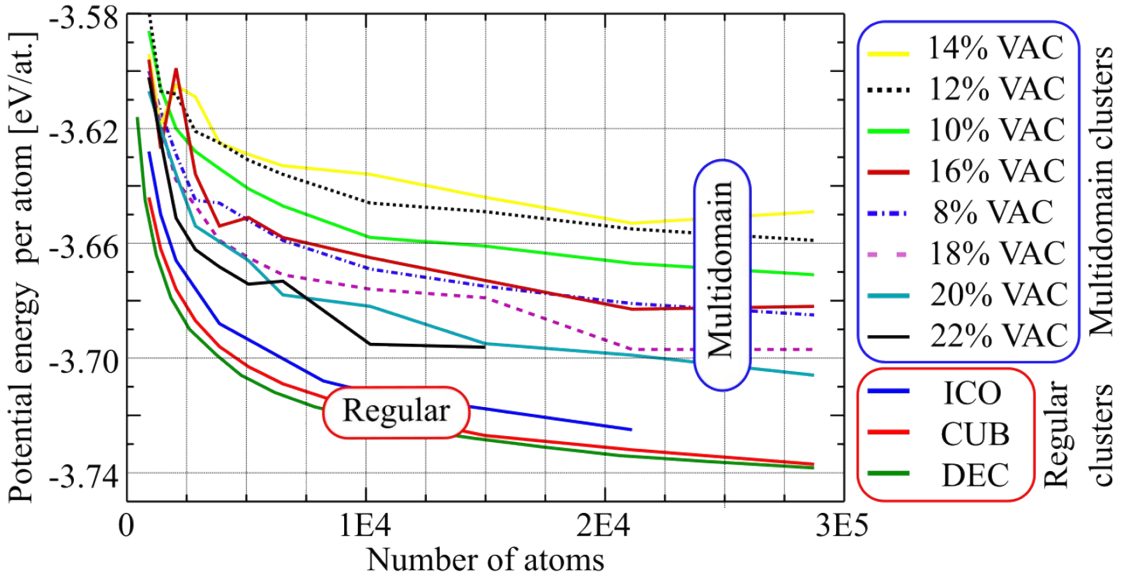

Fig. S3 The minimum potential energy per atom calculated for gold multiply twinned (main article Table 1) and regular CUB, DEC, and ICO nanoparticles as a function of the number of atoms in a cluster. The potential energy was calculated using Cluster software (SC potential).

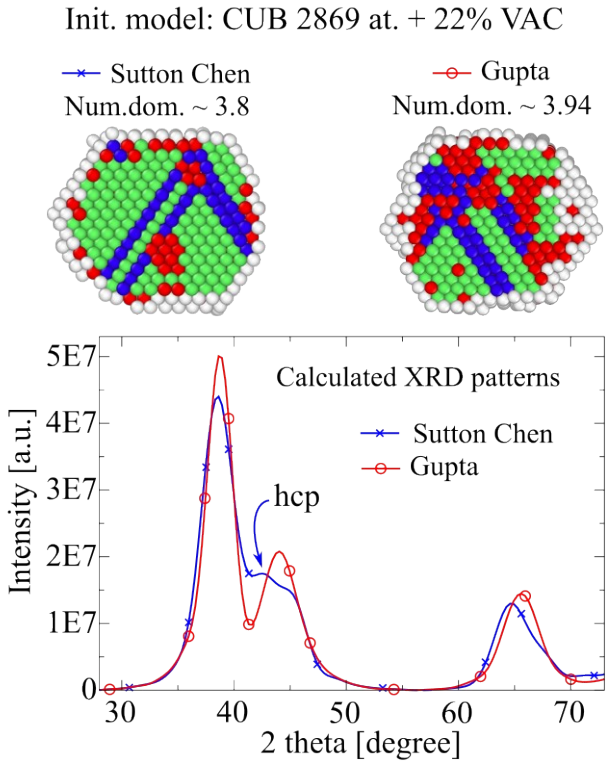

Fig. S4 Comparison of two multidomain models with the same initial state but different potentials used for relaxation: Sutton-Chen (Cluster software) and Gupta potentials.

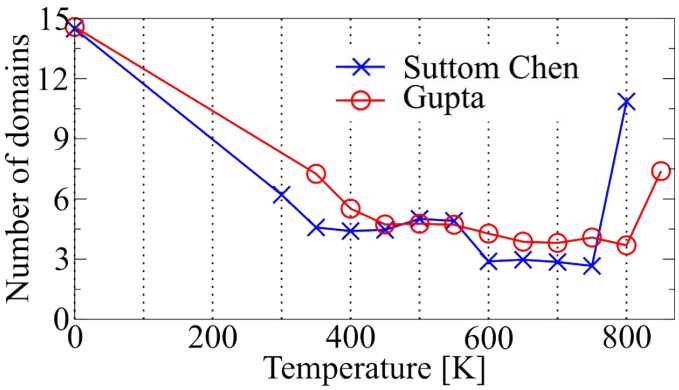

Fig. S5 Evolution of the number of domains in the same multidomain nanoparticle heated using different potentials: the SC potential and the Gupta potential. The initial structure is pre-relaxed (using SC potential) multidomain fcc ball 5089 atoms + 22% of vacancies.

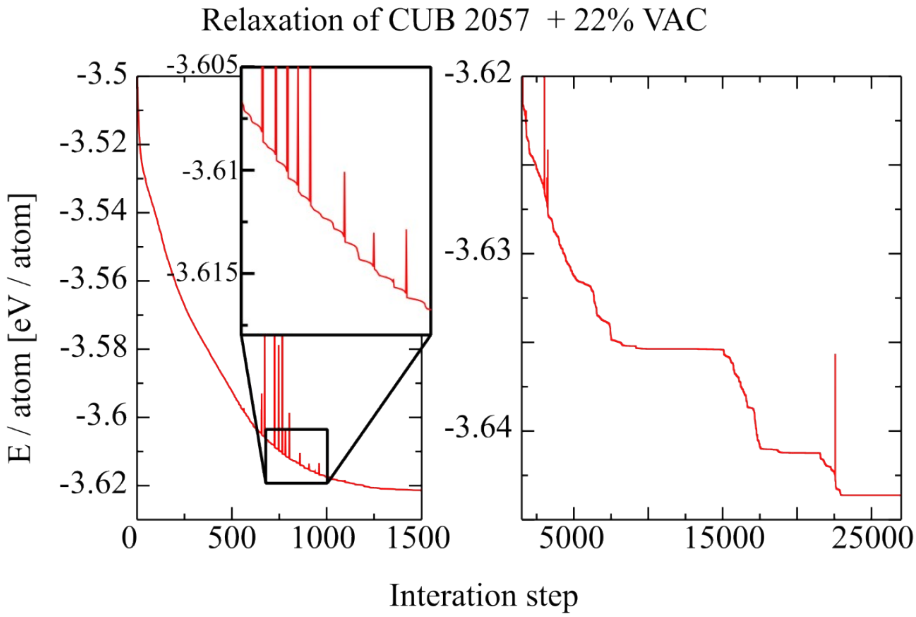

Fig. S6 Evolution of potential energy per atom during relaxation of CUB 2057 with 22% vacancies (SC potential).

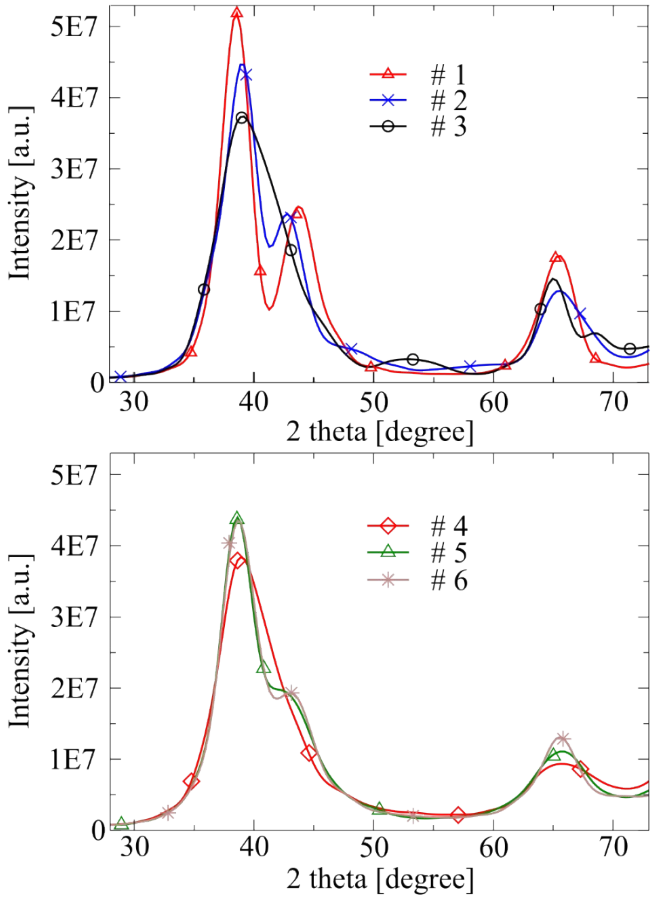

Relaxed CUB 2869 + 22 % VAC

Model	#	111 peak			220 peak			Dom. Num.	Size, nm
		Center	Height	FWHM	Center	Height	FWHM		
CUB 2869 + 22 % VAC	0	38.64	101	3.46	64.81	30	3.68	3.6	4.06
	1	38.55	101	2.91	65.35	33	3.45	2.3	3.75
	2	39.00	95	4.05	65.47	26	3.79	5.1	4.62
	3	39.20	101	5.15	65.05	36	2.97	1.3	3.78
	4	39.07	100	4.76	65.37	18	6.25	13.7	4.00
	5	38.70	99	3.61	65.73	21	5.61	9.4	3.78
	6	38.78	100	3.70	65.58	26	4.19	6.4	4.58
	7	38.56	101	3.05	65.35	29	4.12	4.0	3.72
	9	39.03	96	4.40	66.11	28	3.99	3.3	3.61
	10	39.03	99	4.23	65.04	20	5.87	10.7	3.79
	11	39.03	96	4.39	66.11	28	3.98	3.5	3.69
	12	38.56	101	3.05	65.33	29	4.09	4.0	3.76

Fig. S7 Calculated XRD patterns of the relaxed models (SC potential) having different spatial arrangements of vacancies. All variables were the same; however, the calculated models are different, which can be seen from the corresponding XRD patterns and the table.

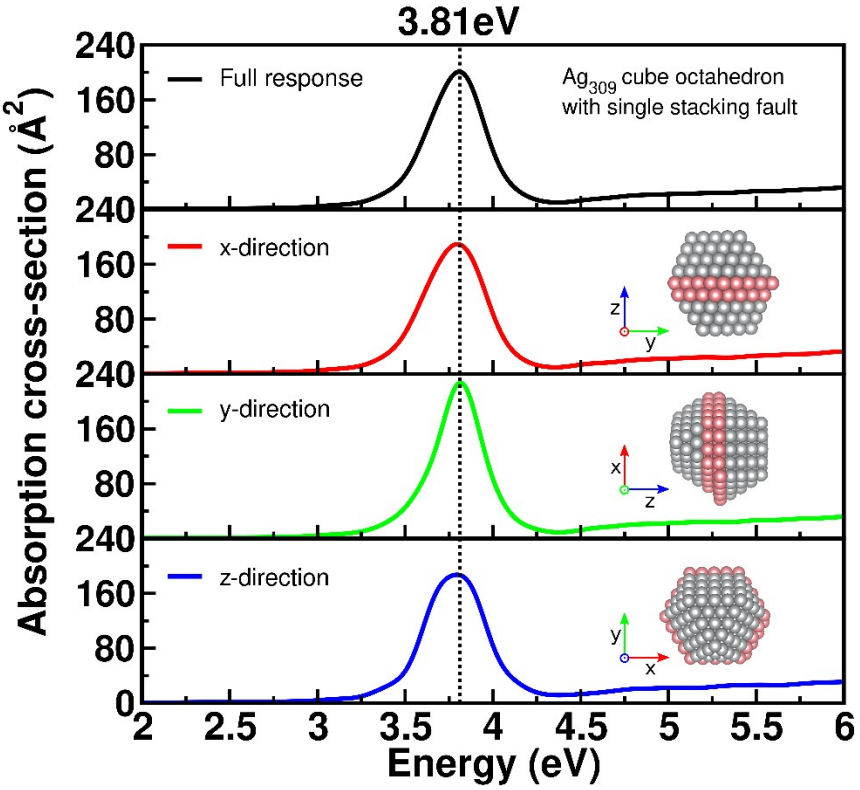

Fig. S8. Direction-resolved absorption spectra of the Ag_{309} cubeoctahedron cluster with a stacking fault show that absorption curves along different directions vary in both width and height of the plasmonic peak, along with a slight difference in peak energy position. Along the direction normal to the plane of the stacking fault (z-direction), the broadening is most pronounced, likely influenced by both the stacking fault and the newly formed edge defects adjacent to the regular fcc domains — an effect that is challenging to decouple in the model.

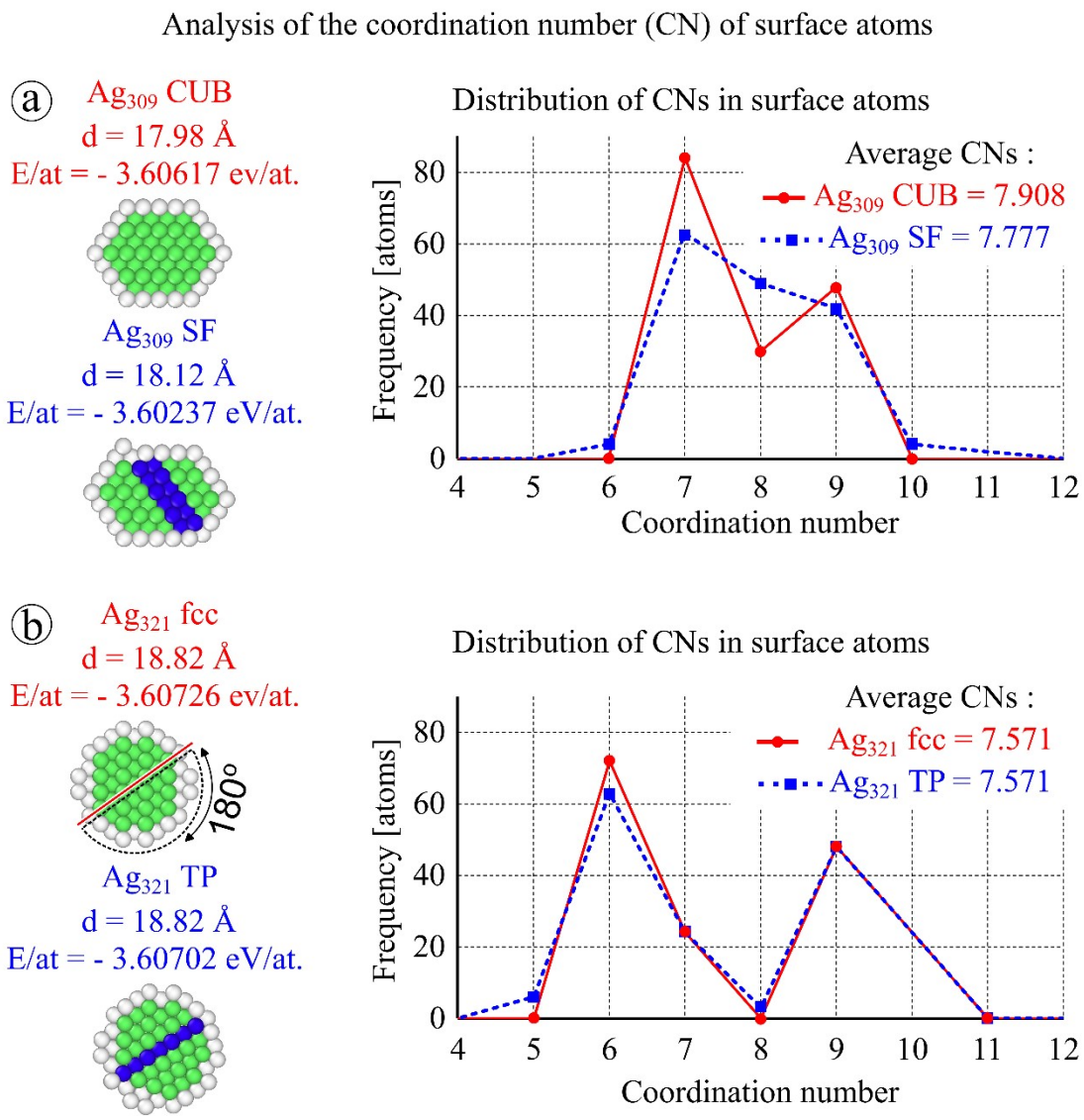

Fig. S9. Shape and Surface Analysis of Regular and Defected Models. Size analysis (performed using Cluster software) is based on identifying surface atoms, calculating the volume, and assuming a spherical shape to determine the diameter. The number of surface atoms remained nearly constant across all models: a) 162 and 164 for Ag_{309} CUB and Ag_{309} SF, respectively; b) 168 atoms for both Ag_{321} fcc and Ag_{321} TP. The energy per atom was calculated for models relaxed using the SC potential. The diagrams on the right of each model represent the coordination number (CN) analysis for surface atoms only. It is evident that the similarity of the energy per atom, shape and surface profile of b) models is significantly greater than the similarity of a) models.

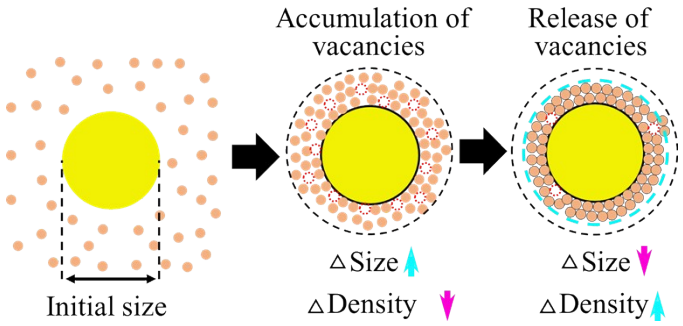

Fig. S10 The scheme of atoms condensation on the seed. While condensing, the newly deposited atoms cannot occupy the optimal position, forming voids/vacancies. After some time, atoms eventually find energetically favorable positions, causing the release of vacancies.

Supplementary Methods

Method S1

The initial nanoparticle structure was created and relaxed using Cluster and then imported as an XYZ file into Blender. Importing the XYZ file is possible thanks to the "PDB/XYZ" add-on. We have found that the "PDB/XYZ" add-on is the most stable for Blender 3.1.2. Some recent versions of Blender may produce incorrect import results.

Once the XYZ file is uploaded into Blender, one can manually adjust the position of each atom or group of atoms ("vertices") in Edit Mode. For example, to create an FCC sphere with a twin plane in the middle (Figure 7b), one needs to select half of the atoms (according to the red line division) and rotate them 180 degrees perpendicular to the twin plane.

To create a CUB-like structure with a stacking fault, a different approach is required. One needs to select a group of atoms (with the middle determined parallel to the (111) planes) and slightly shift them along the x and y coordinates. This modifies the original sequence ABCABCABC to ABCACABCA.

Method S2

To synthesize monometallic, highly disordered nanoparticles, we propose the following methodology. The first step is to prepare a nanoalloy of two immiscible metals, ensuring that the melting temperature of the target metal is at least twice as low as that of the secondary metal. The next step is triggering nanoparticle coalescence and overcoming the threshold at which the alloyed configuration remains stable. Then, the more mobile component (second phase) segregates to the surface, forming voids within the target metal. If the amount of created vacancies exceeds the critical limit, the VDT process will be triggered.

The final step involves the removal of the secondary, mobile phase from the surface, which can be achieved through chemical treatment.

---

[1] Stukowski, A. Visualization and analysis of atomistic simulation data with OVITO–the Open

Visualization Tool. Modelling and Simulation in Materials Science and Engineering 18, 015012 (2009).

[2] Smirnov, I., Kaszkur, Z. & Hoell, A. Development of nanoparticle bulk morphology analysis: a multidomain XRD approach. Nanoscale 15, 8633–8642 (2023).

[3] Rapetti, Daniele, et al. "Machine learning of atomic dynamics and statistical surface identities in gold nanoparticles." Communications Chemistry 6.1 (2023): 143

[4] Cleveland, C. L. et al. Structural Evolution of Smaller Gold Nanocrystals: The Truncated Decahedral Motif. Physical Review Letters 79, 1873–1876 (1997).